EBioMedicine 67 (2021) 103345

Contents lists available at ScienceDirect

EBioMedicine

journal homepage: www.elsevier.com/locate/ebiom

Research paper

Near-infrared photoimmunotherapy targeting human-EGFR in a mouse tumor model simulating current and future clinical trials

Ryuhei Okada[a], Aki Furusawa[a], Daniel W. Vermeer[b], Fuyuki Inagaki[a], Hiroaki Wakiyama[a], Takuya Kato[a], Tadanobu Nagaya[a], Peter L. Choyke[a], William C. Spanos[b,c], Clint T. Allen[d], Hisataka Kobayashi[a,*]

[a] Molecular Imaging Branch, Center for Cancer Research, National Cancer Institute, National Institutes of Health, Bethesda, MD 20892, United States
[b] Cancer Biology Research Center, Sanford Research, Sioux Falls, SD 57104, United States
[c] Department of Surgery, University of South Dakota Sanford School of Medicine, Sioux Falls, SD 57105, United States
[d] Translational Tumor Immunology Program, National Institute on Deafness and Other Communication Disorders, National Institutes of Health, Bethesda, MD 20892, United States

ARTICLE INFO

Article History:
Received 23 February 2021
Revised 31 March 2021
Accepted 1 April 2021
Available online xxx

Keywords:
Photoimmunotherapy
Epidermal growth factor receptor
Regulatory T cell
mEERL

ABSTRACT

Background: near-infrared photoimmunotherapy (NIR-PIT) is a cancer treatment that uses antibody-photoabsorber (IRDye700DX, IR700) conjugates (APCs) which bind to target cells and are photoactivated by NIR light inducing rapid necrotic cell death. NIR-PIT targeting human epidermal growth factor receptor (hEGFR) has been shown to destroy hEGFR expressing human tumor cells and to be effective in immunodeficient mouse models. NIR-PIT can also be targeted to cells in the tumor microenvironment, for instance, CD25-targeted NIR-PIT can be used to selectively deplete regulatory T cells (Tregs) within a tumor. The aim of this study was to evaluate the combined therapeutic efficacy of hEGFR and CD25-targeted NIR-PIT in a newly established hEGFR expressing murine oropharyngeal cell line (mEERL-hEGFR).
Methods: panitumumab conjugated with IR700 (pan-IR700) was used as the cancer cell-directed component of NIR-PIT and anti-CD25-F(ab′)$_2$-IR700 was used as the tumor microenvironment-directed component of NIR-PIT. Efficacy was evaluated using tumor-bearing mice in four groups: (1) non-treatment group (control), (2) pan-IR700 based NIR-PIT (pan-PIT), (3) anti-CD25-F(ab′)$_2$-IR700 based NIR-PIT (CD25-PIT), (4) combined NIR-PIT with pan-IR700 and anti-CD25- F(ab′)$_2$-IR700 (combined PIT).
Findings: the combined PIT group showed the greatest inhibition of tumor growth. Destruction of cancer cells likely leads to an immune response which is amplified by the loss of Tregs in the tumor microenvironment.
Interpretation: combined hEGFR and CD25-targeted NIR-PIT is a promising treatment for hEGFR expressing cancers in which Treg cells play an immunosuppressive role.

1. Introduction

Near-infrared photoimmunotherapy (NIR-PIT) is a newly developed cancer therapy in which an antibody-photoabsorber conjugate (APC) is activated by NIR light at the tumor site [1]. The photoabsorber used in NIR-PIT is a water-soluble silica-phthalocyanine dye, IRDye700DX (IR700), which is readily conjugated to antibodies. After intravenous administration, the APC binds to its target antigen on the cell surface, and subsequent NIR light exposure induces rapid cell specific immunogenic cell death [2,3]. Human epidermal growth factor receptor (hEGFR) is overexpressed on the surface of a variety of cancers, including head and neck, breast, lung, colorectal, prostate, kidney, pancreas, ovary, brain, and bladder cancers [4], and is therefore a good target for NIR-PIT. NIR-PIT not only causes direct cancer cell killing but also induces a strong immune response in the tumor microenvironment (TME) which contributes to effective tumor rejection [5]. A global phase III human clinical trial of NIR-PIT targeting hEGFR in patients with inoperable head and neck cancer is now underway (https://clinicaltrials.gov/ct2/show/NCT03769506). The first drug cetuximab-IR700 (ASP1929) for NIR-PIT has recently been conditionally approved and registered for clinical use by the Pharmaceuticals and Medical Devices Agency (PMDA) in Japan.

Immunosuppressive cells within the TME are particularly promising targets for NIR-PIT. For instance, regulatory T cells (Tregs) play a major role in creating an immune-permissive environment for tumor growth [6]. Selective depletion of intra-tumoral Tregs has been achieved with CD25-targeted NIR-PIT in preclinical models and is

* Corresponding author.
E-mail address: kobayash@mail.nih.gov (H. Kobayashi).

https://doi.org/10.1016/j.ebiom.2021.103345

Research in context

Evidence before this study

Near-infrared photoimmunotherapy (NIR-PIT) is a cell-selective cancer treatment, which uses antibody-photoabsorber conjugate and NIR light. Human epidermal growth factor receptor (hEGFR) targeted NIR-PIT against head and neck cancer was conditionally approved in Japan in September 2020. With appropriate antibody, NIR-PIT could be applied to other types of cells besides cancer cells. In preclinical settings, intratumoral depletion of regulatory T cells (Tregs) has been achieved with CD25-targeted NIR-PIT. Concurrent destruction of cancer cells and intratumoral Tregs by CD44- and CD25-targeted NIR-PIT have been shown to induce superior antitumor efficacy to either monotherapy in mouse models.

Added value of this study

We established a new mouse derived cancer cell line but expressing hEGFR, which is the target molecule for approved NIR-PIT in human patients. Using this cell line and anti-hEGFR antibody, we successfully analyzed the therapeutic efficacy and the immune response of combined NIR-PIT targeting hEGFR and CD25. We showed that the immune response after cancer cell-targeted NIR-PIT and Treg-targeted NIR-PIT were different, yet worked synergically, resulting in potential induction of antitumor immune response, when those two therapies were concurrently performed.

Implications of all the available evidence

This study demonstrated strong antitumor efficacy and feasibility of NIR-PIT concurrently targeting cancer cells and inratumoral Tregs. Combined hEGFR and CD25-targeted NIR-PIT is a promising treatment for hEGFR expressing cancers in which Tregs sufficiently infiltrate.

associated with tumor growth delay or abrogation [7]. CD25 is a component of the IL-2 receptor complex (IL-2Rs) and is expressed on Tregs and activated effector cells, such as $CD8^+$ T cells and natural killer (NK) cells [8–10], though various tumor models have shown that most intra-tumoral $CD25^+$ cells are Tregs [7,11]. Thus, CD25-targeted NIR-PIT selectively depletes Tregs from the TME, resulting in activation of effector cells and upregulation of antitumor immunity [7,12]. As there is concern about depletion of effector T cells due to antibody-dependent cellular cytotoxicity (ADCC)/complement-dependent cytotoxicity (CDC), the Fc region of anti-CD25-IgG was removed and a truncated antibody [anti-CD25-F(ab′)$_2$] was used in the APC. The smaller size of the F(ab′)$_2$ also results in more rapid clearance and less blocking of IL-2/IL-2R binding on effector cells, which contribute to improved effector T cell proliferation [12].

Near-infrared photoimmunotherapy can concurrently destroy multiple cell types if multiple APCs are injected. For example, combined CD44- and CD25-targeted NIR-PIT has been shown to kill both cancer cells and Tregs, resulting in greater immune activation and inhibition of tumor growth than either therapy alone [13]. However, CD44 is expressed on both cancer cells and immune cells [5], thus, CD44-targeted NIR-PIT might reduce antitumor immunity and is, therefore, not an ideal model to analyze the additional effect of CD25-targeted NIR-PIT.

In this study we established mEERL-hEGFR cells which are a modified mEERL cell line. The parental mEERL (mEERL-WT) cells are transduced with the human papillomavirus 16 (HPV16) E6 and E7 oncogenes and the mEERL-hEGFR line is further transduced with hEGFR. hEGFR is not expressed on natural murine cells, therefore, hEGFR-targeted NIR-PIT against mEERL-hEGFR tumor does not cause off-target effect to other murine cells. The aim of this study was first to evaluate the efficacy of hEGFR-targeted NIR-PIT in this new syngeneic model of head and neck cancers, mEERL-hEGFR. Subsequently, the anti-cancer effects of combined hEGFR- and CD25-targeted NIR-PIT in the same model were evaluated in immunocompetent mice.

2. Methods

2.1. Reagents

IR700 NHS ester was obtained from LI-COR Biosciences (Lincoln, NE, USA; cat # 929-70011). Panitumumab was purchased from Amgen (Thousand Oaks, CA, USA; RRID AB_2459650). Anti-mouse CD25 antibody (clone PC-61.5.3; cat # BE0012) was purchased from Bio X Cell (West Lebanon, NH, USA). Anti-CD25-F(ab′)$_2$ was manufactured from anti-CD25-IgG as previously described [7]. All other chemicals were of reagent grade.

2.2. Synthesis of antibody-photoabsorber conjugate (APC)

Panitumumab (1 mg, 6.8 nmol) or anti-CD25-F(ab′)$_2$ (1 mg, 9.1 nmol) was incubated with 5-fold molar excess of IR700 NHS ester in phosphate buffer (pH 8.5) at room temperature for 1 h. The mixture was purified with a Sephadex G25 column (PD-10; GE Healthcare, Piscataway, NJ, USA). The APCs are referred to as pan-IR700 and anti-CD25-F(ab')2-IR700, respectively.

2.3. Cell lines

mEERL-WT cells were established by transduction of HPV 16 E6/E7 and hRAS to C57BL/6-derived oropharyngeal epithelial cells [14–16]. mEERL-hEGFR cells were established by stable transformation of mEERL cells with hEGFR as follows. Briefly, hEGFR from a plasmid stock was cloned utilizing the In-Fusion HD Cloning Kit (Clontech; cat # 102518) into a previously generated pBabe plasmid construct with a zeocin resistance cassette. After sequence verification of the pBabe hEGFRzeo construct, retrovirus was generated from Phoenix-AMPHO cells (ATTC CRL-3213) by transfection with polyfect (Qiagen; cat # 301107) per the manufacturer's directions. Parental mEERL cells were then transduced with the retrovirus and placed under zeocin selection (500 μg/mL), uninfected control cells died and clonal lines were derived from single cells in the retrovirus infected population. A clonal mEERL-hEGFR cell line was selected based on hEGFR messenger RNA expression, protein expression, and growth *in vivo*. Reverse transcription polymerase chain reaction (RT-PCR) was performed with the primers, (Fwd: ACACCTGCCCCCCACTCATG and Rev: CGCCACTGATGGAGGTGCAG) identifying a hEGFR product of 318 bp. *In vitro* surface expression of hEGFR was evaluated with immunofluorescence staining using Erbitux (Eli Lilly &Co., Indianapolis, IN, USA) and AlexaFluor 488 (Invitrogen; cat # A11013) secondary antibody. DAPI was used for counter staining nuclei. *In vivo* hEGFR expression was assessed by immunohistochemical staining with anti-hEGFR (clone EGFR.1; BD biosciences; cat # 555996) and anti-activated hEGFR (clone 13/EGFR; BD biosciences; cat # 610025). These cells were newly made by our own and authenticated with mouse short-tandem repeat profiling service by ATCC. Both cell lines were cultured in DMEM/F-12 medium (Thermo Fisher Scientific, Waltham, MA, USA; cat # 1320033) supplemented with 10% fetal bovine serum (Thermo Fisher Scientific; cat # 16000044), 1% penicillin/streptomycin (Thermo Fisher Scientific; cat # 15140122) and 1× human keratinocyte growth supplement (Thermo Fisher Scientific; cat # S0015), which was modified from a previous report [17]. Cells were cultured in a humidified incubator at 37 °C in an atmosphere of 95% air and 5% CO_2.

2.4. Cell-specific binding analysis

mEERL-WT/hEGFR cells were collected with trypsin (Thermo Fisher Scientific; cat # 15400054) and two hundred cells were aliquoted in 100 μL volume PBS. To test panitumumab binding, cells were incubated with 1 μg of panitumumab in 100 μL PBS for 1 h at 4 °C followed by incubation with anti-human IgG-PE (Thermo Fisher Scientific; cat # 12-4998-82, 1:100 dilution) for 30 minutes at 4 °C. To test pan-IR700 binding, cells were incubated with 1 μg of pan-IR700 in 100 μL PBS for 1 h at 4 °C. To confirm the specific binding of the pan-IR700, 10-fold excess of panitumumab was added to some samples 1 h prior to the administration of the pan-IR700. Fluorescence of the cells was analyzed with a flow cytometer (FACSLyric, BD Biosciences, San Jose, CA, USA) and FlowJo software (BD Biosciences).

2.5. In vitro *NIR-PIT*

Twenty thousand cells of mEERL-WT/hEGFR were seeded into glass bottomed 35 mm dish. After one day, the cells were incubated with 10 μg/mL of pan-IR700 for 1 h at 37 °C. After washing with PBS, phenol-red-free medium was added. The cells were then exposed to NIR light (690 nm, 150 mW/cm^2, 50 J/cm^2) with an ML7710 laser system (Modulight, Tampere, Finland). Transmitted light differential interference contrast (DIC) images were obtained before and after the light exposure with a microscope (IX81; Olympus America, Melville, NY, USA). For quantitative assessment of the cytotoxicity, three hundred thousand cells of mEERL-WT or mEERL-hEGFR were seeded into 12-well plates. NIR-PIT was performed as same as above. NIR light (690 nm, 150 mW/cm^2) was applied at 0, 1, 4, 16, and 64 J/cm^2. One hour after the light exposure, the cells were collected with trypsin and stained with 1 μg/mL propidium iodide (PI). The percentage of PI-stained cells were analyzed with flow cytometry.

2.6. Animals and tumor models

All *in vivo* procedures were conducted in compliance with the Guide for the Care and Use of Laboratory Animal Resources (1996), US National Research Council, and approved by the local Animal Care and Use Committee (MIP-003; project number P183735). Six- to eight-week-old female C57BL/6 mice were purchased from The Jackson Laboratory (Bar Harbor, ME, USA). One million mEERL-hEGFR cells were inoculated into the right side of the dorsum. The hair overlying the tumor site was removed for the light exposure and the imaging studies. Tumor volume was calculated as (major axis) $\times$ (minor axis)$^2 \times 0.5$. Tumor volumes were measured twice a week until the volume reached 1000 mm^3, whereupon the mice were euthanized with CO_2.

2.7. In vivo *fluorescence imaging*

Pan-IR700 (100 μg) was injected via lateral tail vein 6 days after inoculation of the tumor. Serial dorsal fluorescence images were taken with the 700-nm fluorescence channel of a Pearl Imager (LI-COR Bioscience). The images were obtained before and 1, 3, 6, 9, 12, 24, 48, 72, and 96 h after injection of the pan-IR700. The images were analyzed with Pearl Cam Software (LI-COR Bioscience). Regions of interest (ROIs) were drawn on the tumor and the non-tumoral region of the contralateral side. Target-to-background ratio was calculated as (Mean fluorescence intensity of the tumor)/(Mean fluorescence intensity of a normal region of the contralateral side).

2.8. In vivo *NIR-PIT*

In order to evaluate the *in vivo* efficacy of hEGFR-targeted NIR-PIT, tumor-bearing mice were randomized into 3 groups as follows: (1) no treatment (control), (2) intravenous administration of pan-IR700 (100 μg) without NIR light exposure (pan-IR700-IV), and (3) intravenous administration of pan-IR700 (100 μg) followed by NIR light exposure (pan-PIT). In order to evaluate the efficacy of combined hEGFR and CD25-targeted NIR-PIT, tumor-bearing mice were randomized into 4 groups; (1) no treatment (control), (2) intravenous administration of pan-IR700 (50 μg) followed by NIR light exposure (pan-PIT), (3) intravenous administration of anti-CD25-F(ab′)$_2$-IR700 (50 μg) followed by NIR-light exposure (CD25-PIT), and (4) intravenous administration of both pan-IR700 and anti-CD25-F(ab′)$_2$-IR700 (50 μg per each) followed by NIR-light exposure (combined PIT). Mice with ulcerating tumor were excluded from the study. The APCs were injected 6 days after the inoculation of tumor. The exposure to NIR light (690 nm, 150 mW/cm^2, 50 J/cm^2) was performed at the timings indicated. Anti-mouse CD8 (clone YTS 169.4; cat # BE0117) or its corresponding isotype control (rat IgG2b, clone LTF-2; cat # BE0090) from Bio X Cell was intraperitonially injected (200 μg, twice a week, three weeks) to see the efficacy of NIR-PIT under the CD8$^+$ cell depletion.

2.9. Flow-cytometric analysis

Tumors were digested with collagenase type IV (1 mg/mL; Thermo Fisher Scientific; cat # 17104019) and DNase I (20 μg/mL; cat # 11284932001; Millipore Sigma, Burlington, MA, USA), then dissociated and filtered with 70 μm cell strainer (Corning, Corning, NY, USA; cat # 431751). The cells were stained with antibodies purchased either from Biolegend [anti-CD3e (clone 145−2C11; cat # 100306), anti-CD8α (clone 53−6.7; cat # 100734), anti-CD31(clone 390; cat # 102420), anti-CD45 (clone 30F-11; cat # 103108), and anti-hEGFR (clone AY13; cat # 352903) or its corresponding isotype control (clone MOPC-21; cat # 400114)] or from Thermo Fisher Scientific [anti-CD4 (clone RM4−5; cat # 14-0042-85), anti-CD25 (clone PC61.5; cat # 17-0251-82), anti-CD44 (clone IM7; cat # 12-0441-83), anti-CD62L (clone MEL-14; cat # 17-0621-82), and anti-NK1.1 (clone PK136; cat # 45-5941-82)]. To distinguish live cells, the cells were also stained with LIVE/DEAD Fixable Dead Cell Stain (Thermo Fisher Scientific; cat # L-34974) or Fixable Viability Dye (Thermo Fisher Scientific; cat # 65-0866-14). For the staining of Foxp3, the cells were fixed and permeabilized with Foxp3 Transcription Factor Staining Buffer set (Thermo Fisher Scientific; cat # 00-5523-00) followed by the incubation with anti-Foxp3 (clone FJK-16s; Thermo Fisher Scientific; cat # 17-5773-82). The stained cells were analyzed with FACSCalibur or FACSLyric flow cytometer and FlowJo software.

2.10. Tetramer assay

Tumor draining lymph nodes were harvested 7 days after the treatment and processed into single cell suspensions via mechanical crushing. After filtration (70 μm), cells (1×10^6 cells) were aliquoted for staining. Cells were incubated with anti-mouse CD16/32 (clone 93; Biolegend; cat # 101301) to reduce non-specific staining. Cells were sequentially stained with iTag H-2Db HPV 16 E7 (RAHYNIVTF; cat # TB-5008-1), H-2Kb p15E (KSPWFTTL; cat # TB-M507-1) or H-2Kb Ova (SIINFEKL; cat # TB-5001-1) tetramers (MBL International, Woburn, MA, USA) for 30 min, followed by staining with anti-mouse CD45.2 (clone 104; cat # 109815) from Biolegend and anti-CD8 (clone KT15; cat # D271-A64) from MBL. Dead cells were excluded on analysis following sytox blue (Thermo Fisher Scientific; cat # S34857) staining. Isotype control antibodies and fluorescence-minus-one approaches were used to ensure staining specificity. All analyses were performed on a BD Fortessa analyzer running FACSDiva software and interpreted using FlowJo (vX10.0.7r2).

2.11. Multicolor immunofluorescence staining

Multicolor immunofluorescence staining was performed to analyze the tumor-infiltrating lymphocytes (TILs) as previously described [12,13]. The sections were stained with DAPI and the following antibodies: anti-CD8 (clone EPR20305; Abcam, Cambridge, UK; cat # ab209775; 1:500 dilution), anti-CD4 (clone EPR 19514; Abcam; cat # ab221775; 1:1000 dilution), anti-Foxp3 (clone 1054C; Novus Biologicals, Centennial, CO, USA; cat # MAB8214; 1:1000 dilution), and anti-pan cytokeratin (rabbit poly; Bioss Antibodies, Woburn, MA, USA; cat # bs-1712R; 1:250 dilution). Tissue area was divided into "Tumor" and "Stroma" based on the expression of pan cytokeratin. Four pictures were obtained for each specimen, and tissue area and cell count were summed for each tissue category. Cell density was calculated as cell counts per square millimeter.

2.12. Statistical analysis

Data are expressed as means ± SEM. Statistical analysis was performed with GraphPad Prism (GraphPad Software, La Jolla, CA, USA). For a comparison of mean fluorescence intensity of anti-hEGFR and that of isotype control, a paired *t*-test was used. For multiple-group comparison with one-time measurement, a one-way analysis of variance (ANOVA) followed by Tukey's test was used. For comparison of tumor volumes, a repeated measures two-way ANOVA followed by Sidak's test (two groups) or Tukey's test (three or more groups) was used. The cumulative probability of survival based on tumor volume (1000 mm^3) was estimated with the Kaplan-Meier survival curve analysis, and the results were compared with log-rank test with Bonferroni correction. *p*-value of less than 0.05 was considered significant.

2.13. Role of funding source

No funding source had role in the study design, data collection, data analysis, interpretation, or writing of the manuscript.

3. Results

3.1. Generation of hEGFR expressing murine cancer model

hEGFR was introduced into the mEERL (mEERL-WT) cell line [14–16] using viral transduction. After single cell cloning, hEGFR expression was evaluated with RT-PCR and immunofluorescence staining (Supplementary Fig. 1(a) and (b)). Two selected clones, #11 and #12, were inoculated into C57BL/6 mice. Although both cell lines established tumors, immunohistochemical staining against hEGFR revealed that only #11 expressed hEGFR in established tumors (Supplementary Fig. 1(c)). Thus, #11 was used for further experiments and this cell line is referred to as mEERL-hEGFR.

3.2. Panitumumab NIR-PIT kills mEERL-hEGFR cells but not mEERL-WT cells

In this study, panitumumab, a fully humanized IgG2 monoclonal antibody binding to hEGFR, was used for cancer cell targeting. Panitumumab binding to mEERL-hEGFR cell line was confirmed with flow cytometry (Supplementary Fig. 2). Next, to verify the binding of the panitumumab-IR700 conjugate (pan-IR700) to mEERL-hEGFR cells, flow cytometry was performed. mEERL-WT cells showed no fluorescent signal after one-hour incubation with pan-IR700. On the other hand, mEERL-hEGFR cells showed fluorescence, which was blocked with excess non-conjugated panitumumab suggesting specific binding (Fig. 1(a)). To evaluate the *in vitro* cell killing efficacy of NIR-PIT with pan-IR700 (pan-PIT), both cell lines were incubated with pan-IR700 for one hour and then exposed to NIR light. Cell morphology was microscopically examined. mEERL-WT showed no obvious changes, while mEERL-hEGFR showed cellular swelling, bleb formation and rupture of cell membrane immediately after the light exposure (Fig. 1(b)). The cell killing efficacy of NIR-PIT was quantitatively assessed with flow cytometry by PI staining (Fig. 1(c)). The percentage of dead cells increased after pan-PIT in mEERL-hEGFR cells in a light dose dependent manner, whereas no such increase was observed in mEERL-WT cells. The administration of pan-IR700 alone or exposure to NIR light alone did not affect cell viability.

3.3. *hEGFR is expressed* in vivo *on mEERL-hEGFR tumors*

To verify the *in vivo* expression of hEGFR, established tumors were removed and single cell suspensions were made and then analyzed with flow cytometry (Fig. 1(d)). Only CD31-CD45- cells, which included mEERL-hEGFR cells, showed hEGFR expression. $CD31^+CD45^-$ endothelial cells or $CD45^+$ hematopoietic cells did not express hEGFR. These results suggested pan-PIT selectively kills mEERL-hEGFR cells, but not endothelial cells or immune cells within the TME. To assess the accumulation of pan-IR700 within the tumor, serial fluorescence images were obtained in live tumor bearing mice (Supplementary Fig. 3(a)). The peak average fluorescence of the tumor was shown around 6–12 h after the injection of pan-IR700, then it gradually decreased (Supplementary Fig. 3(b)). Target-to-background ratios also showed the same trend (Supplementary Fig. 3(c)).

3.4. In vivo *NIR-PIT targeting hEGFR inhibits mEERL-hEGFR tumor growth*

The treatment effect of pan-PIT in mEERL-hEGFR tumors was evaluated *in vivo*. The treatment effect was compared in three groups of animals: no treatment (control), pan-IR700 injection without NIR light exposure (pan-IR700-IV), and pan-IR700 injection followed by NIR light exposure (pan-PIT). The NIR light was administered twice to the tumor (Supplementary Fig. 4(a)). Fluorescence at 700 nm confirmed the accumulation of pan-IR700 within the tumor (Supplementary Fig. 4(b)). This fluorescence immediately decreased after NIR light exposure due to photobleaching of IR700. The fluorescence reaccumulated by the next day and but decreased again after the second exposure to NIR light. These changes in fluorescence demonstrated that a sufficient light flux was administered to cause photochemical changes in IR700. The tumor growth was significantly inhibited in the pan-PIT group compared to the other two groups, while pan-IR700-IV group showed no significant effect on tumor growth inhibition (Supplementary Fig. 4(c)). The pan-PIT group achieved significantly prolonged survival compared to the control group (Supplementary Fig. 4(d)). In order to compare histology after NIR-PIT, the tumors were harvested 1 h after light exposure. The injection of pan-IR700 without light exposure induced no obvious histological changes. On the other hand, in the pan-PIT group, swelling and vacuolation of the tumor cells was observed, indicating necrotic death of the tumor cells (Supplementary Fig. 4(e)).

3.5. CD25 is expressed mainly on Tregs

In order to assess what cell populations could be destroyed by CD25-targeted NIR-PIT, expression of CD25 in established mEERL-hEGFR tumors was analyzed with flow cytometry. $Foxp3^+$ Tregs accounted for 49.8% on average of $CD3^+CD4^+$ T cells, which suggested Tregs were plentiful in the tumor (Fig. 2(a)). Conversely, 71.5% of CD25 positive cells were $CD3^+CD4^+Foxp3^+$ Tregs (Fig. 2(b)). The expressions of CD25 on NK cells, $CD8^+$ T cells, $CD4^+Foxp3^-$ T cells, and $CD4^+Foxp3^+$ Tregs were compared (Fig. 2(c)). Among these cells, Tregs showed significantly higher mean fluorescence intensity (MFI) and CD25 positive percentage than the other types of cells. These results suggested that CD25-targeted NIR-PIT destroys mainly Tregs within the TME.

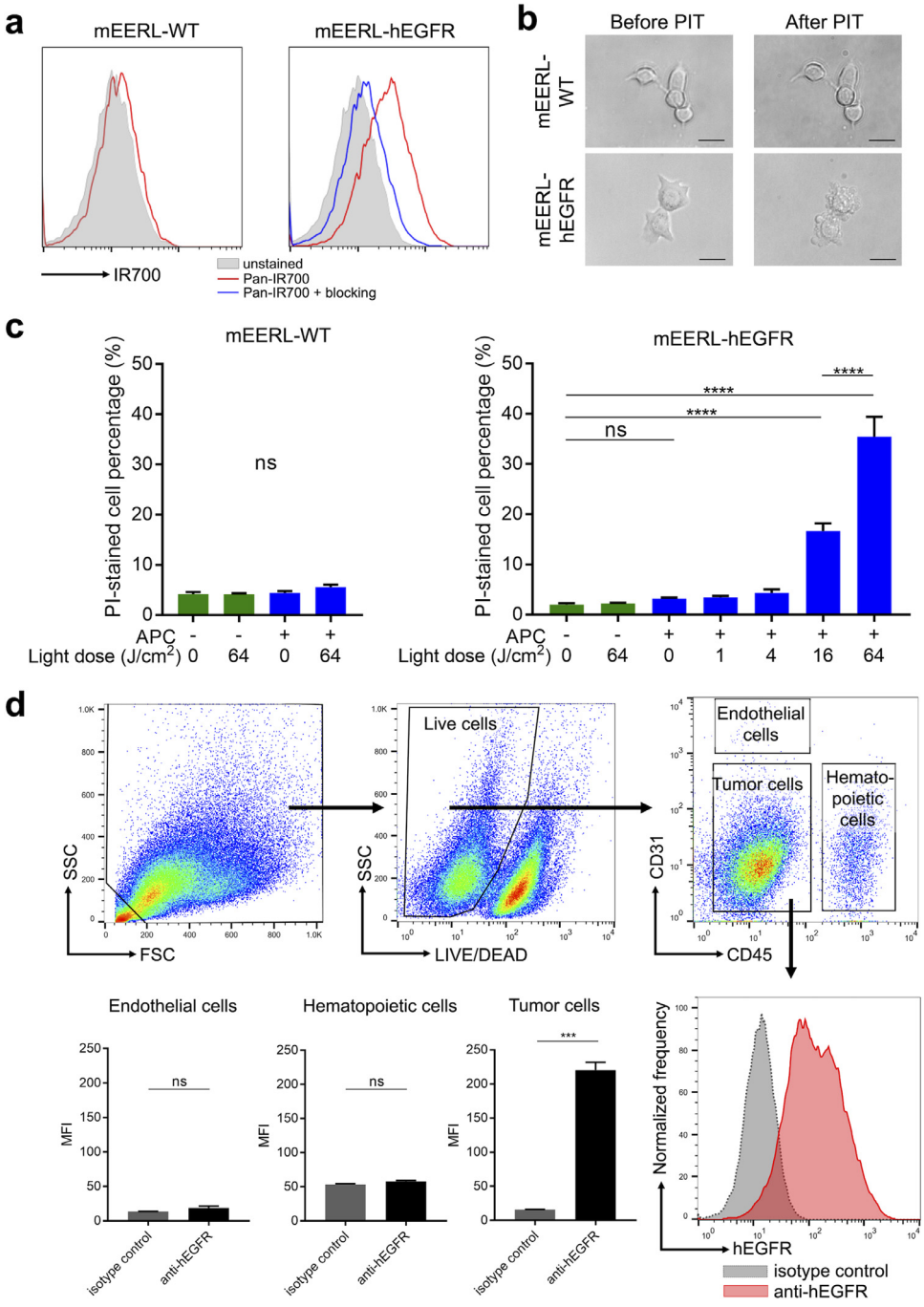

Fig. 1. Characteristics of the mEERL-hEGFR cell line. **(a)** mEERL-hEGFR cells showed a fluorescent shift compared to unstained cells after incubation with pan-IR700 by flow cytometry. **(b)** Microscopic observation of the cells before and after NIR-PIT. Panitumumab based NIR-PIT killed mEERL-hEGFR cells. Scale bar, 20 μm. **(c)** Quantitative cytotoxicity assay with flow cytometry. Panitumumab based NIR-PIT showed no cytotoxicity to mEERL-WT cells, while it killed mEERL-hEGFR cells in a light dose dependent manner ($n = 4$; one-way ANOVA followed by Tukey's test; ****, $p < 0.0001$; ns, not significant). **(d)** *In vivo* hEGFR expression was assessed with flow cytometry. Gating strategy of analysis of hEGFR expression. Dead cells were removed from the analysis based on the values of FSC, SSC, and viability dye staining. The live cells were classified into endothelial cells, hematopoietic cells, and tumor cells according to the expression of CD45 and CD31. Only the tumor cell population showed hEGFR expression ($n = 4$; paired t-test; ***, $p < 0.001$; ns, not significant; vs. isotype control).

3.6. Combined NIR-PIT targeting hEGFR and CD25 inhibits tumor growth more than either therapy alone

Next, we tested the efficacy of the combined NIR-PIT targeting hEGFR and CD25. We assessed if CD25-targeted NIR-PIT (CD25-PIT) affects mEERL-hEGFR cells *in vitro* where there is no TME. For CD25-PIT, IR700 conjugated anti-CD25-F(ab′)$_2$ [anti-CD25-F(ab′)$_2$-IR700] was used. Cultured mEERL-hEGFR cells were incubated with anti-CD25-F(ab′)$_2$-IR700, yet the cells showed no increase of fluorescence (Supplementary Fig. 5(a)). Also, *in vitro* CD25-PIT did not destroy mEERL-hEGFR cells (Supplementary Fig. 5(b)). These results indicated that CD25 is not expressed on mEERL-hEGFR cells therefore CD25-PIT does not affect these cells. Then, we compared pan-PIT alone (pan-PIT) CD25-PIT alone (CD25-PIT), and both pan-PIT and CD25-PIT (combined PIT) in the context of *in vivo* NIR-PIT with non-treatment control group. The treatment and imaging regimen are shown in Fig. 3(a). For all NIR-PIT groups, the 700-nm fluorescence was clearly observed at the tumor site prior to NIR light exposure. This

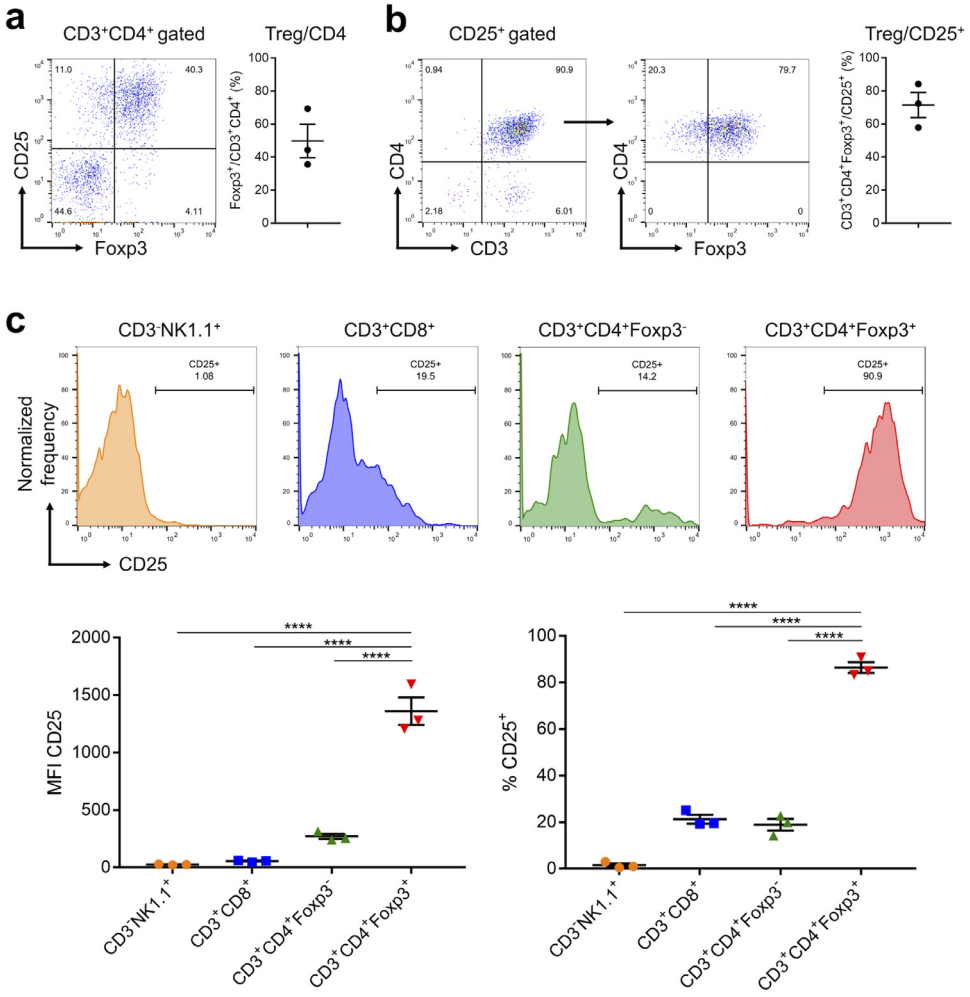

Fig. 2. CD25 expression on tumor-infiltrating lymphocytes. **(a)** Tumor-infiltrating lymphocytes were analyzed with flow cytometry. Tregs accounted for 49.8% of $CD4^+$ T cells. **(b)** 71.5% of CD25 positive cells were $CD3^+CD4^+Foxp3^+$ Tregs **(c)** Upper: Surface expression of CD25 was evaluated for NK cells, $CD8^+$ T cells, $CD4^+Foxp3^-$ T cells, and $CD4^+Foxp3^+$ Tregs. Lower: $CD4^+Foxp3^+$ Tregs showed significantly higher mean fluorescence intensity (MFI) of CD25 (left) and CD25 positive percentage (right) ($n = 4$; one-way ANOVA followed by Tukey's test; ****, $p < 0.0001$).

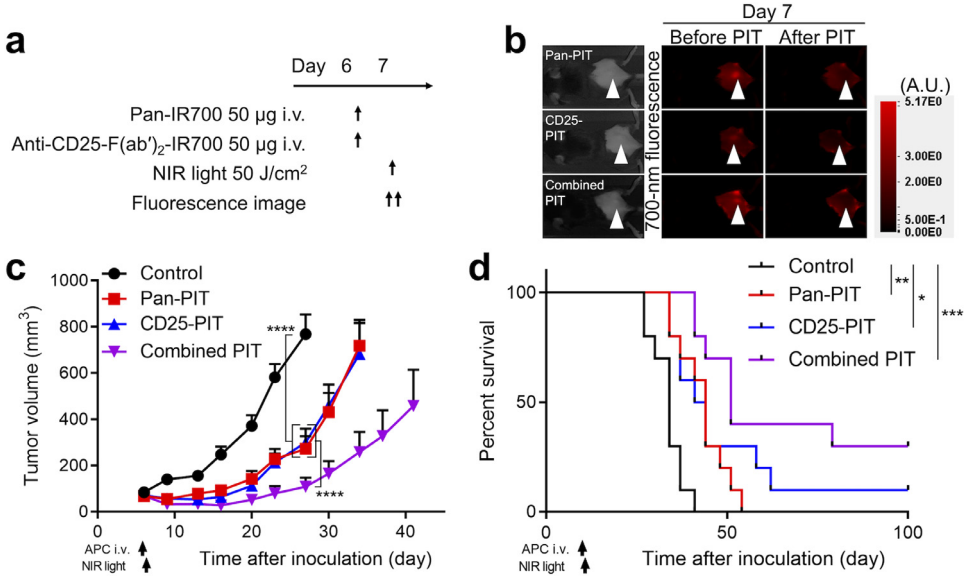

Fig. 3. *In vivo* efficacy of combined NIR-PIT targeting hEGFR and CD25. **(a)** Treatment schedule. **(b)** The fluorescence of the tumor decreased immediately after light exposure. White arrowheads represent the locations of tumors. A.U., arbitrary unit. **(c)** Tumor volume curves ($n = 10$; repeated measures two-way ANOVA followed by Tukey's test; ****, $p < 0.0001$). **(d)** Survival curves ($n = 10$; log-rank test with Bonferroni correction; *, $p < 0.05$, **, $p < 0.01$, ***, $p < 0.001$). The CD25-PIT and the combined PIT cleared the tumor in 1/10, 3/10 mice, respectively.

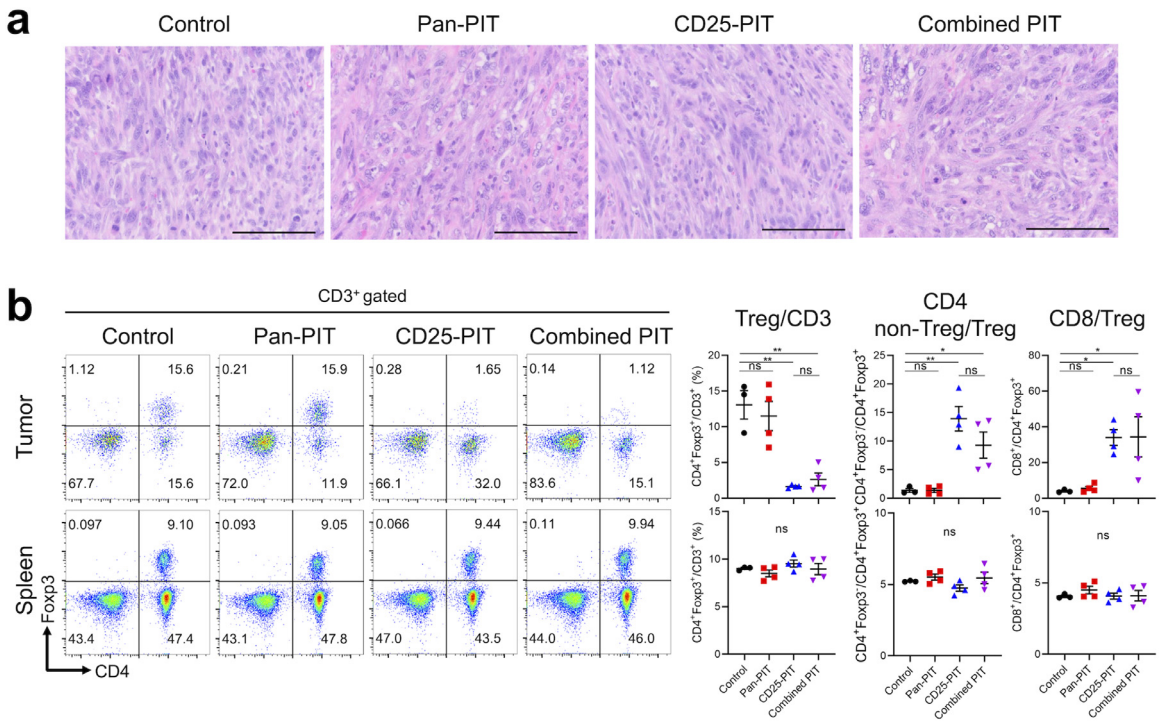

Fig. 4. Selective cell destruction by *in vivo* NIR-PIT. **(a)** Histological evaluation with H-E stained section. Scale bar represents 100 μm. Pan-PIT group and combined PIT group induced swelling and vacuolation of the tumor cells within 1 h after the light exposure. **(b)** Lymphocytes within tumor and spleen were analyzed with flow cytometry 1 h after each therapy. The dot plots show the representative expression of CD4 and Foxp3 among $CD3^+$ T cells. The scatter plots show the percentages of Tregs in $CD3^+$ T cells, ratios of non-regulatory/regulatory $CD4^+$ T cells ($CD4^+Foxp3^-/CD4^+Foxp3^+$), and ratios of $CD8^+$ T cells/Tregs ($CD8^+/CD4^+Foxp3^+$). ($n = 3-4$; one-way ANOVA followed by Tukey's test; *, $p < 0.05$; **, $p < 0.01$; ns, noT significant).

fluorescence immediately decreased after NIR light exposure, indicating that a sufficient dose of light was administered to cause photobleaching of the IR700 dye (Fig. 3(b)). All the NIR-PIT groups significantly suppressed tumor growth compared with the control group and the efficacy was prominent in the combined PIT group, which suppressed tumor growth more compared to either monotherapy (Fig. 3(c), Supplementary Fig. 6). Furthermore, all the PIT groups achieved significantly prolonged survival compared to the control group (Fig. 3(d)). Although the survival of the combined PIT group was not significantly prolonged compared to either monotherapy, combined PIT cleared a larger number of the tumors (3 of 10) than pan-PIT (0 of 10) or CD25-PIT (1 of 10) monotherapy. The histological changes at one hour after the light exposure were compared among the four groups (Fig. 4(a)). Both pan-PIT and combined PIT induced tumor cell swelling and vacuolation, while no obvious histological change was shown for CD25-PIT. To assess if the CD25-PIT and combined PIT deplete the Tregs within the TME, T cell populations were analyzed by flow cytometry at 1 h after the NIR light irradiation to the tumor (Fig. 4(b)). In these two groups, intratumoral $CD4^+Foxp3^+$ Tregs were successfully depleted from $CD3^+$ T cells, resulting in increased $CD4^+$ non-Treg/Treg ratio and $CD8^+$/Treg ratio, which are known to be an indicator of robust antitumor immune response [18,19]. On the other hand, these changes were not shown in the spleen which was not exposed to light. These results suggested that CD25-PIT depletes the Tregs only at the targeted site receiving light exposure. To assess if the combined PIT shows abscopal effect, bilateral tumor model was used. mEERL-hEGFR cells were inoculated into the both dorsi but only the right side was exposed to NIR light (Supplementary Fig. 7(a–c)). Combined PIT against the right sided tumor induced the tumor growth suppression of the contralateral tumor, suggesting combined NIR-PIT induces abscopal effect (Supplementary Fig. 7(d)). The antitumor efficacy of combined PIT group was significantly attenuated by $CD8^+$ cell depletion indicating this effect is $CD8^+$ cell dependent (Supplementary Fig. 8), therefore, we further analyzed the immune reaction after the therapy.

3.7. *CD25-PIT leads to accumulation of $CD8^+$ T cells in tumor tissue*

The infiltration of $CD8^+$ T cells in tumor is an important indicator of antitumor immune reaction. To assess the accumulation of $CD8^+$ T cells in TME after each therapy, tumor tissue was extracted one week after the treatment and stained with multiplex immunohistochemical staining (Fig. 5(a)). $CD8^+$, $CD4^+Foxp3^-$, and $CD4^+Foxp3^+$ cells were counted for each specimen. $CD8^+$ cells showed a significantly higher density in the CD25-PIT group and in the combined PIT group compared to the control group (Fig. 5(b)), resulting in higher $CD8^+$/Treg ratios (Fig. 5(c)).

3.8. *CD25-targeted NIR-PIT causes $CD8^+$ T cells to differentiate into memory T cells*

To assess the differentiation of the $CD8^+$ T cell in the regional lymph node, ipsilateral inguinal lymph nodes were extracted one week after the treatment. $CD8^+$ T cells were classified into naïve T cells + stem cell memory T (T_{SCM}) cells, central memory T (T_{CM}) cells, effector memory T (T_{EM}) cells, and effector T cells according to their expression of CD44 and CD62L (Supplementary Fig. 9(a)) [20,21]. All the PIT groups (*i.e.* pan-PIT group, CD25-PIT group, and combined PIT group) showed a significantly higher percentage of T_{CM} than the non-treatment control group, and the percentage of T_{CM} in the CD25-PIT group and the combined PIT group was significantly higher than that of the pan-PIT group (Supplementary Fig. 9(b)). These results suggest CD25-PIT induces $CD8^+$ T cells in tumor draining lymph nodes to differentiate into memory T cells.

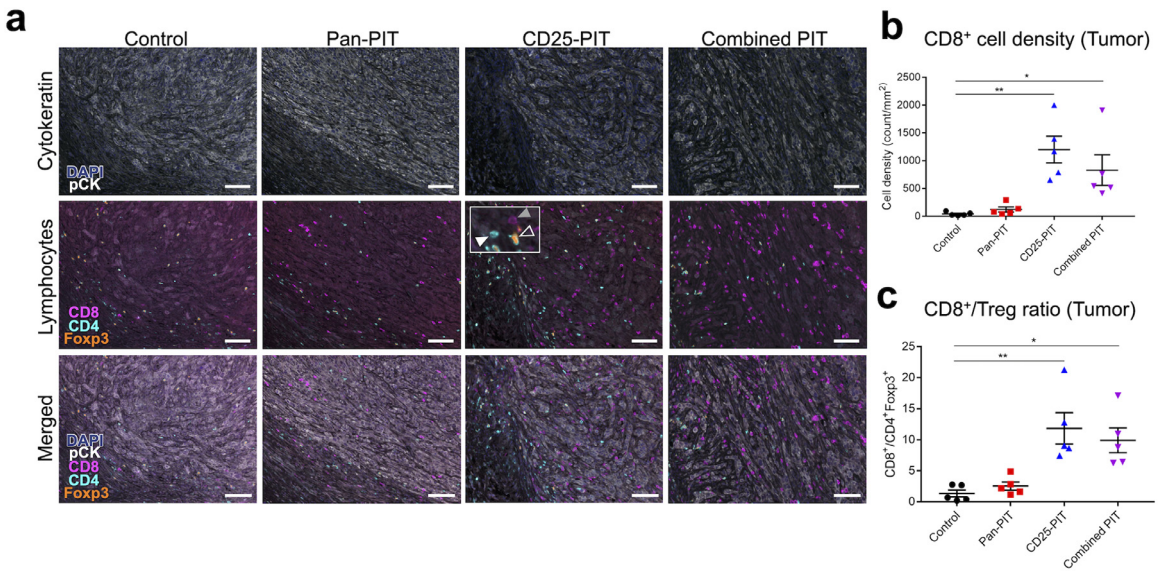

Fig. 5. CD8$^+$ cell accumulation into the tumor. **(a)** Multiplex immunohistochemical staining of the tumors 7 days after the therapy. Top: cytokeratin staining to mark tumor tissue. Middle: lymphocyte marker staining; CD8 (magenta), CD4 (cyan) and Foxp3 (orange). The inset in the picture of CD25-PIT shows examples of CD8$^+$ cell (gray filled arrowhead), CD4$^+$Foxp3$^-$ cell (white filled arrowhead) and CD4$^+$Foxp3$^+$ cell (open arrowhead). bottom: merged image. Scale bar, 100 μm. **(b)** intratumoral CD8$^+$ cell density was significantly higher in the CD25-PIT group and the combined PIT group than the control group ($n = 5$; one-way ANOVA followed with Tukey's test; *, $p < 0.05$, **, $p < 0.01$). **(c)** intratumoral CD8$^+$/CD4$^+$Foxp3$^+$ (Treg) ratio was also increased in these two groups compared with the control group ($n = 5$; one-way ANOVA followed with Tukey's test; *, $p < 0.01$; **, $p < 0.05$). (For interpretation of the references to color in this figure legend, the reader is referred to the web version of this article.)

3.9. Tumor-targeted NIR-PIT prompts host immunity to recognize tumor-associated antigens

To assess if proliferated CD8$^+$ T cells recognize tumor-associated antigens, ipsilateral inguinal lymph nodes were harvested one week after the treatment. The percentage of CD8$^+$ T cells among CD45$^+$ cells was significantly higher in nodes from the combined PIT group compared with the other groups (Fig. 6(a)). Tumor-specificity was evaluated with tumor specific tetramers (Fig. 6(b)). mEERL is transduced by HPV 16 E7 with retrovirus so that HPV 16 E7 tetramer and retrovirus protein p15E tetramer were used as known tumor antigens. Ova tetramer was used for negative control. In the control group, few CD8$^+$ T cells bound to E7 tetramer and CD25-PIT group showed no evidence of an increase T cells binding E7. However, the Pan-PIT group significantly increased the population of E7 binding T cells and this was further increased in the combined PIT group (Fig. 6(c)). The same trend was also demonstrated in p15E tetramer, though even control groups showed measurable binding. These results suggest that tumor-targeted NIR-PIT prompts recognition of tumor-associated antigens by the host immune system and it is enhanced by combination with Treg-targeted NIR-PIT.

3.10. Combined NIR-PIT results in immunologic memory

To assess the presence of immunologic memory, mice rejected the tumor by combined NIR-PIT were re-inoculated with the mEERL-hEGFR cells ten weeks after the therapy on the contralateral dorsum (Supplementary Fig. 10(a) and 10(b)). Although control mice were engrafted, the mice once completely cleared the tumor by the combined NIR-PIT rejected re-engrafment (Supplementary Fig. 10(c) and (d)). These results suggest immunologic memory was developed after the combined NIR-PIT.

4. Discussion

We established a unique immunocompetent mouse tumor model for simulating the effects of hEGFR-targeted NIR-PIT and demonstrated that the combination of hEGFR- and CD25-targeted NIR-PIT is more effective than either treatment alone. Although a previous study has shown that CD44- and CD25-targeted NIR-PIT was highly effective in mouse models [13], that result was clouded by the fact that CD44- is expressed on both cancer cells and lymphoid cells. The mEERL-hEGFR model with hEGFR and CD25 targeting is ideal because there is no overlap between the cell types to which the two antibodies bind. The mEERL-hEGFR cells were verified to express hEGFR but not CD25 on their surface by flow cytometry. hEGFR-targeted *in vitro* NIR-PIT induced rapid cell death. Based on flow cytometry of established tumors, only the CD45$^-$CD31$^-$ population, which includes mEERL-hEGFR cells, demonstrated cell-surface hEGFR expression, while CD31$^+$ CD45$^-$ endothelial cells or CD45$^+$ hematopoietic cells showed no evidence of its expression. Thus, hEGFR-targeted NIR-PIT selectively destroyed mEERL-hEGFR cells without cytotoxicity to endothelial cells or hematopoietic cells. Meanwhile CD25-targeted NIR-PIT mainly targeted Tregs. The combination appeared to be more successful than either method alone.

Currently, three monoclonal antibodies targeting hEGFR, cetuximab, panitumumab, and necitumumab, have been approved by the FDA for hEGFR-expressing cancers. Among these, cetuximab and panitumumab have been widely used for over 10 years [22]. In the mouse model, panitumumab has a longer half-life than cetuximab, and thus panitumumab based NIR-PIT showed greater antitumor effect than cetuximab based therapy [23]. Panitumumab was therefore used in this study for targeting tumor cells. In the *in vivo* fluorescence study to assess the biodistribution, the fluorescent signal derived from pan-IR700 was clearly detected as early as one hour after the injection and had its peak within 24 h after intravenous administration, which matches the data of pan-IR700 for hEGFR-expressing human cancers in athymic nude mice [23]. Therefore, approximately one day after injection is the most appropriate time to apply NIR light to the tumor.

It is important to note that the anti-hEGFR antibody alone did not have a therapeutic effect on the tumor because the transfected hEGFR is not thought to be biologically active and therefore its inhibition is not therapeutic [24,25]. Also, ADCC induced by pan-IR700 is likely weaker in mice than in humans. Human IgG2, which is the isotype of panitumumab, has been reported to bind murine FcγRIIb and FcγIII

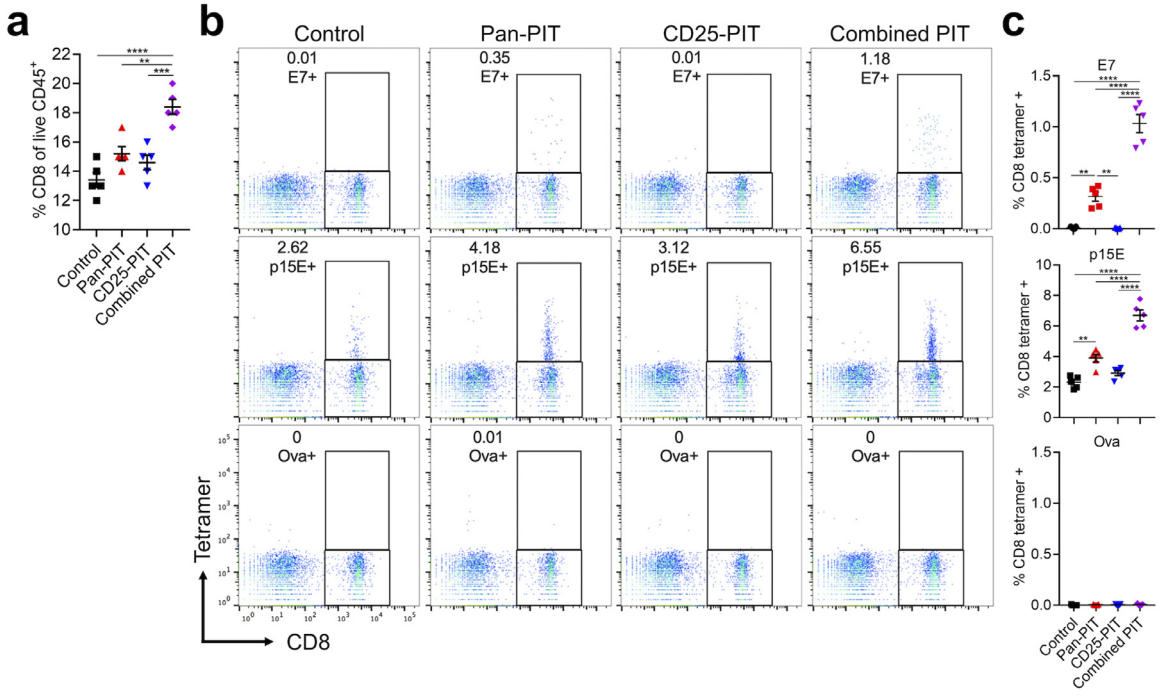

Fig. 6. Tetramer assay for tumor draining lymph node. **(a)** Tumor draining lymph nodes were analyzed 7 days after each therapy. The percentage of $CD8^+$ cells among $CD45^+$ cells was assessed with flowcytometry ($n = 5$; one-way ANOVA followed with Tukey's test,;**, $p < 0.01$; ***, $p < 0.001$; ****, $p < 0.0001$). **(b)** Tetramer binding population among $CD8^+$ cell was evaluated. Ova tetramer was used for negative control. **(c)** HPV 16 E7 tetramer biding percentage was significantly higher in pan-PIT group compared with control and CD25-PIT group. In the combined PIT group, it was higher than in the pan-PIT group. Similarly, p15E tetramer binding percentage was significantly higher in the pan-PIT group than in the control group and it was further higher in the combined PIT group ($n = 5$; one-way ANOVA followed with Tukey's Test; **, $p < 0.01$; ****$p < 0.0001$).

inducing ADCC with murine NK cells and polymorphonuclear leukocytes (PMNs), and less so with macrophages [26,27]. However, binding affinity to the activating FcγIII and inhibitory FcγRIIb are similar [26] so that ADCC induced by panitumumab tends to be weak in mice. Moreover, the drug dose used in this study was probably not high enough for antitumor effects. In this study, 100 μg of APC was administrated, which is lower than previous reports that showed the efficacy of panitumumab against hEGFR-expressing human carcinoma using the athymic nude mice [28,29]. In this study, panitumumab was used only for targeting the cancer cell; neither inhibition of the hEGFR signaling pathway nor ADCC was necessary for the therapy to be effective, and this selective cancer cell destruction was achieved with low dose of the drug.

It is challenging to simulate the human TME in mouse models. The mEERL-hEGFR model is useful because most CD25 expressing cells were $CD4^+Foxp3^+$ Tregs, and Tregs expressed CD25 at a frequency of over 80%. In contrast, few effector cells (*e.g.*, NK cells, $CD8^+$ T cells, and $CD4^+Foxp3^-$ T cells) overexpressed CD25. This agrees with the literatures in which effector cells tend to express less CD25 than Tregs within most tumors [7,11]. Moreover, CD25-targeted NIR-PIT had no impact on the peripheral Treg population outside the range of NIR light exposure, which was confirmed with splenocyte analysis. Systemic administration of anti-CD25-IgG reportedly depletes peripheral Tregs [30], which may induce autoimmune adverse events [31–33]. CD25-targeted NIR-PIT depletes Tregs only at the tumor site where NIR light is exposed and could therefore be a safer method than systemic Treg depletion.

NIR-PIT targeting both hEGFR and CD25 successfully killed both cancer cells and Tregs within the TME, as confirmed by histological analysis and flow cytometry, resulting in improved tumor growth suppression. These results suggest that concurrent destruction of the cancer cells and Tregs induces a stronger immune reaction than either NIR-PIT monotherapy (Fig. 7). Multiplex immunohistochemical staining of tumor tissue 7 days after the therapy supported this conclusion. CD25-targeted NIR-PIT and combined NIR-PIT led to the accumulation of $CD8^+$ T cells in the TME, resulting an increased $CD8^+$/Treg ratio. $CD8^+$ T cells in tumor draining lymph nodes were also analyzed. Naïve T cells differentiate into stem cell memory T (T_{SCM}) cells, followed, in order, by central memory T (T_{CM}) cells, effector memory T (T_{EM}) cells, and then effector T cells [34,35]. Naïve T cells, T_{SCM} cells, and T_{CM} cells express lymphoid homing receptors, such as CD62L and CCR7, and localize to secondary lymphoid organs, whereas, T_{EM} cells and effector T cells which lack these receptors accumulate in peripheral tissues [35–37]. T_{CM} cells could be distinguished from Naïve T cells and T_{SCM} cells using their high expression of CD44 [38]. In this study, all three PIT groups (pan-PIT, CD25-PIT, and combined PIT group) showed a significantly higher percentage of T_{CM} cells among $CD8^+$ T cells than the untreated control group, and the increase in CD25-PIT group and combined PIT group were significantly greater than the pan-PIT group. These results suggest that the cancer cell-targeted NIR-PIT prompts $CD8^+$ T cells to differentiate into memory T cells and Treg-targeted NIR-PIT promotes this differentiation stronger than the cancer cell-targeted NIR-PIT. The establishment of memory T cell population is favorable for long-term antitumor immunity. According to the results of the tetramer assay, T cells with tumor-associated tetramer binding, which specifically react to mEERL-hEGFR cells, was significantly greater in pan-PIT group and was further enhanced by combination with CD25-PIT whereas CD25-PIT alone did not show such increase. These results indicate that the cancer cell-targeted NIR-PIT induced specific antitumor immune reaction and Treg-targeted NIR-PIT enhanced it. Also, immunogenic memory was developed by combined NIR-PIT resulted in rejection of re-engraftment. We believe cancer cell-targeted NIR-PIT induces not only direct cancer cell killing but also an antitumor immune reaction by releasing many kinds of tumor-associated antigens that are recognized by host immune cells. The effects of cancer cell-targeted NIR-PIT and Treg-targeted NIR-PIT are different but complementary to each other, resulting in an effective antitumor immune reaction

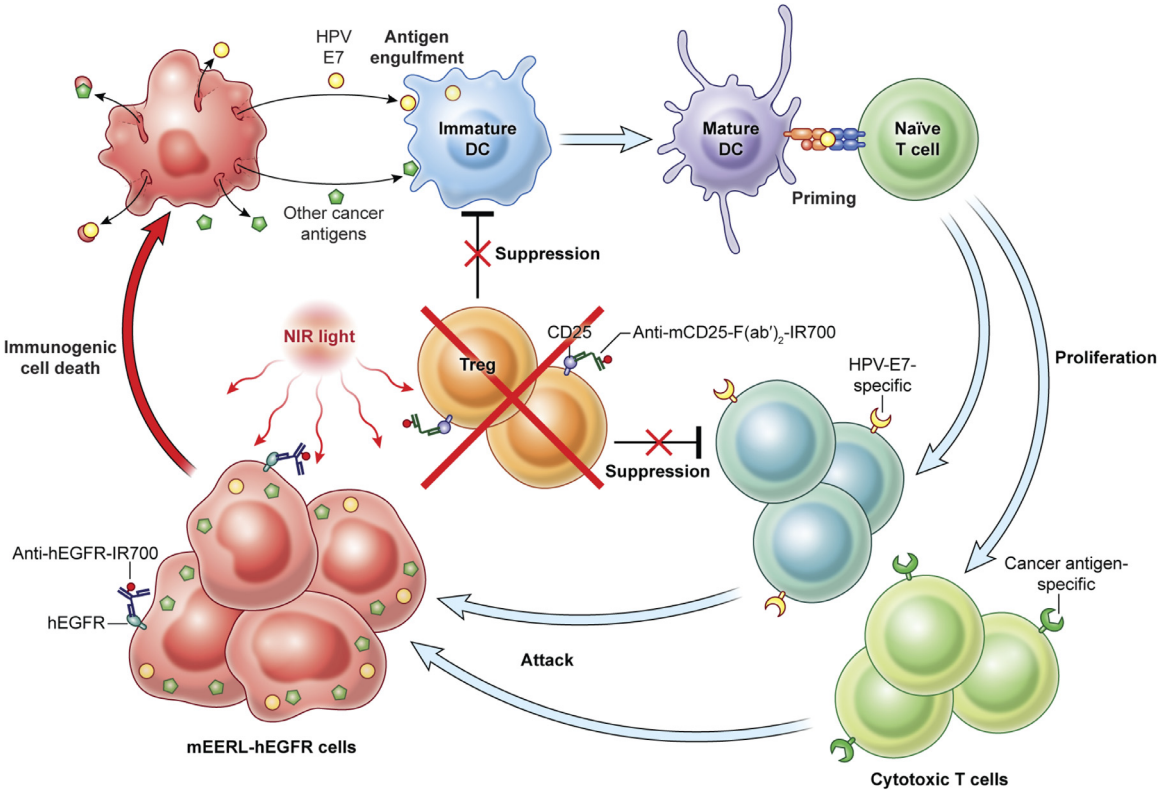

Fig. 7. Scheme indicates the proposed mechanism of combined NIR-PIT concurrently targeting hEGFR and CD25 against mEERL-hEGFR tumor. hEGFR-targeted NIR-PIT induces immunogenic cell death of mEERL-hEGFR cancer cells, promoting tumor-associated antigen presentation to dendritic cells. CD25-targeted NIR-PIT attenuates the intratumoral immunosuppression mediated by Tregs, inducing proliferation and activation of cytotoxic T cells.

when those therapies are concurrently combined. hEGFR is overexpressed on the surface of a variety of cancers. Therefore, hEGFR-targeted NIR-PIT has therapeutic potential against a broad array of tumors. However, there are many other target molecules overexpressed on cancer cells, such as human epidermal growth factor receptor 2 (HER2), mesothelin, programmed death-ligand 1 (PD-L1), CD20, prostate-specific membrane antigen (PSMA) that are amenable to NIR-PIT [39–43]. Therefore, combined cancer cell/Treg targeted NIR-PIT could be applied broadly to various kind of tumors.

There are several limitations to this study. First, hEGFR expression is not very high in the mEERL-hEGFR cell line. Higher expression of the hEGFR might have led to greater efficacy for panitumumab-based NIR-PIT monotherapy. Second, hEGFR itself may serve as a tumor neoantigen in the murine system. However, tumor growth suggested it is not highly reactive. Third, we used only one cell line in this study largely because such murine models are very unique and difficult to develop. The results may be different in other cancers. Nonetheless mEERL-hEGFR tumor is successfully established as a mouse tumor model for simulating the clinical setting of hEGFR-targeted NIR-PIT. NIR-PIT targeting both hEGFR and CD25 successfully killed cancer cells and Tregs inducing a strong immune reaction which was highly effective. Due to the selective expression of the targets, the effects were independent but complementary to each other. Therefore, selective destruction of cancer cells and immunosuppressive cells with NIR-PIT could be successfully applied to a wide variety of cancers.

Author contributions

All authors read and approved the final version of the manuscript. R.O. mainly designed and conducted experiments, performed analysis, verifying data and wrote the manuscript; A.F., F.I., H.W., T.K., and T.N. performed experiments and analysis; D.W.V and W.C.S developed the human EGFR construct and cells, reviewed data and the manuscript; C.T.A. designed and conducted experiments and performed analysis; P.L.C. wrote the manuscript and supervised the project; and H.K. planned and initiated the project, designed and conducted experiments, verifying data, wrote the manuscript, and supervised the entire project.

Data sharing section

Publicly created datasets or codes are not available.

Declaration of Competing Interest

The authors have no conflict of interest to disclose. W.C.S. has performed consulting with Regeneron, BMS, Ambu with no overlap with this project.

Acknowledgements

This research was supported by the Intramural Research Program of the National Institutes of Health, National Cancer Institute, Center for Cancer Research (ZIA BC011513) and National Institute on Deafness and Other Communication Disorders (ZIA-DC00008). F.I. was also supported with a grant from National Center for Global Health and Medicine Research Institute, Tokyo, Japan.

Supplementary materials

Supplementary material associated with this article can be found, in the online version, at doi:10.1016/j.ebiom.2021.103345.

References

[1] Mitsunaga M, Ogawa M, Kosaka N, Rosenblum LT, Choyke PL, Kobayashi H. Cancer cell-selective *in vivo* near infrared photoimmunotherapy targeting specific membrane molecules. Nat Med 2011;17:1685–91.

[2] Ogawa M, Tomita Y, Nakamura Y, Lee MJ, Lee S, Tomita S, et al. Immunogenic cancer cell death selectively induced by near infrared photoimmunotherapy initiates host tumor immunity. Oncotarget 2017;8:10425–36.

[3] Sato K, Ando K, Okuyama S, Moriguchi S, Ogura T, Totoki S, et al. Photoinduced ligand release from a silicon phthalocyanine dye conjugated with monoclonal antibodies: a mechanism of cancer cell cytotoxicity after near-infrared photoimmunotherapy. ACS Cent Sci 2018;4:1559–69.

[4] Martinelli E, De Palma R, Orditura M, De Vita F, Ciardiello F. Anti-epidermal growth factor receptor monoclonal antibodies in cancer therapy. Clin Exp Immunol 2009;158:1–9.

[5] Nagaya T, Friedman J, Maruoka Y, Ogata F, Okuyama S, Clavijo PE, et al. Host immunity following near-infrared photoimmunotherapy is enhanced with PD-1 checkpoint blockade to eradicate established antigenic tumors. Cancer Immunol Res 2019;7:401–13.

[6] Nishikawa H, Sakaguchi S. Regulatory T cells in cancer immunotherapy. Curr Opin Immunol 2014;27:1–7.

[7] Sato K, Sato N, Xu B, Nakamura Y, Nagaya T, Choyke PL, et al. Spatially selective depletion of tumor-associated regulatory T cells with near-infrared photoimmunotherapy. Sci Transl Med 2016;8:352ra110.

[8] Spolski R, Li P, Leonard WJ. Biology and regulation of IL-2: from molecular mechanisms to human therapy. Nat Rev Immunol 2018;18:648–59.

[9] Liao W, Lin JX, Leonard WJ. Interleukin-2 at the crossroads of effector responses, tolerance, and immunotherapy. Immunity 2013;38:13–25.

[10] Sakaguchi S, Sakaguchi N, Asano M, Itoh M, Toda M. Immunologic self-tolerance maintained by activated T cells expressing IL-2 receptor alpha-chains (CD25). Breakdown of a single mechanism of self-tolerance causes various autoimmune diseases. J Immunol 1995;155:1151–64.

[11] Arce Vargas F, Furness AJS, Solomon I, Joshi K, Mekkaoui L, Lesko MH, et al. Fc-optimized anti-CD25 depletes tumor-infiltrating regulatory T cells and synergizes with PD-1 blockade to eradicate established tumors. Immunity 2017;46:577–86.

[12] Okada R, Maruoka Y, Furusawa A, Inagaki F, Nagaya T, Fujimura D, et al. The effect of antibody fragments on CD25 targeted regulatory T cell near-infrared photoimmunotherapy. Bioconjug Chem 2019;30:2624–33.

[13] Maruoka Y, Furusawa A, Okada R, Inagaki F, Fujimura D, Wakiyama H, et al. Combined CD44- and CD25-targeted near-infrared photoimmunotherapy selectively kills cancer and regulatory T cells in syngeneic mouse cancer models. Cancer Immunol Res 2020;8:345–55.

[14] Hoover AC, Spanos WC, Harris GF, Anderson ME, Klingelhutz AJ, Lee JH. The role of human papillomavirus 16 E6 in anchorage-independent and invasive growth of mouse tonsil epithelium. Arch Otolaryngol Head Neck Surg 2007;133:495–502.

[15] Spanos WC, Hoover A, Harris GF, Wu S, Strand GL, Anderson ME, et al. The PDZ binding motif of human papillomavirus type 16 E6 induces PTPN13 loss, which allows anchorage-independent growth and synergizes with ras for invasive growth. J Virol 2008;82:2493–500.

[16] Williams R, Lee DW, Elzey BD, Anderson ME, Hostager BS, Lee JH. Preclinical models of HPV+ and HPV- HNSCC in mice: an immune clearance of HPV+ HNSCC. Head Neck 2009;31:911–8.

[17] Mermod M, Hiou-Feige A, Bovay E, Roh V, Sponarova J, Bongiovanni M, et al. Mouse model of postsurgical primary tumor recurrence and regional lymph node metastasis progression in HPV-related head and neck cancer. Int J Cancer 2018;142:2518–28.

[18] Quezada SA, Peggs KS, Curran MA, Allison JP. CTLA4 blockade and GM-CSF combination immunotherapy alters the intratumor balance of effector and regulatory T cells. J Clin Invest 2006;116:1935–45.

[19] Quezada SA, Peggs KS, Simpson TR, Allison JP. Shifting the equilibrium in cancer immunoediting: from tumor tolerance to eradication. Immunol Rev 2011;241:104–18.

[20] Zoon CK, Wan W, Graham L, Bear HD. Addition of interleukin-21 for expansion of T-cells for adoptive immunotherapy of murine melanoma. Int J Mol Sci 2015;16:8744–60.

[21] Zoon CK, Wan W, Graham L, Bear HD. Expansion of T cells with interleukin-21 for adoptive immunotherapy of murine mammary carcinoma. Int J Mol Sci 2017;18.

[22] Tebbutt N, Pedersen MW, Johns TG. Targeting the ERBB family in cancer: couples therapy. Nat Rev Cancer 2013;13:663–73.

[23] Sato K, Watanabe R, Hanaoka H, Harada T, Nakajima T, Kim I, et al. Photoimmunotherapy: comparative effectiveness of two monoclonal antibodies targeting the epidermal growth factor receptor. Mol Oncol 2014;8:620–32.

[24] Jakobovits A, Amado RG, Yang X, Roskos L, Schwab G. From XenoMouse technology to panitumumab, the first fully human antibody product from transgenic mice. Nat Biotechnol 2007;25:1134–43.

[25] Saltz L, Easley C, Panitumumab Kirkpatrick P. Nat Rev Drug Discov 2006;5:987–8.

[26] Overdijk MB, Verploegen S, Ortiz Buijsse A, Vink T, Leusen JH, Bleeker WK, et al. Crosstalk between human IgG isotypes and murine effector cells. J Immunol 2012;189:3430–8.

[27] Steplewski Z, Sun LK, Shearman CW, Ghrayeb J, Daddona P, Koprowski H. Biological activity of human-mouse IgG1, IgG2, IgG3, and IgG4 chimeric monoclonal antibodies with antitumor specificity. Proc Natl Acad Sci USA 1988;85:4852–6.

[28] Yang XD, Jia XC, Corvalan JR, Wang P, Davis CG, Jakobovits A. Eradication of established tumors by a fully human monoclonal antibody to the epidermal growth factor receptor without concomitant chemotherapy. Cancer Res 1999;59:1236–43.

[29] Yang XD, Jia XC, Corvalan JR, Wang P, Davis CG. Development of ABX-EGF, a fully human anti-EGF receptor monoclonal antibody, for cancer therapy. Crit Rev Oncol Hematol 2001;38:17–23.

[30] Setiady YY, Coccia JA, Park PU. *In vivo* depletion of CD4+FOXP3+ Treg cells by the PC61 anti-CD25 monoclonal antibody is mediated by FcgammaRIII+ phagocytes. Eur J Immunol 2010;40:780–6.

[31] Taguchi O, Takahashi T. Administration of anti-interleukin-2 receptor alpha antibody *in vivo* induces localized autoimmune disease. Eur J Immunol 1996;26:1608–12.

[32] Facciabene A, Motz GT, Coukos G. T-regulatory cells: key players in tumor immune escape and angiogenesis. Cancer Res 2012;72:2162–71.

[33] Caspi RR. Immunotherapy of autoimmunity and cancer: the penalty for success. Nat Rev Immunol 2008;8:970–6.

[34] Farber DL, Yudanin NA, Restifo NP. Human memory T cells: generation, compartmentalization and homeostasis. Nat Rev Immunol 2014;14:24–35.

[35] Klebanoff CA, Gattinoni L, Restifo NP. CD8+ T-cell memory in tumor immunology and immunotherapy. Immunol Rev 2006;211:214–24.

[36] Sallusto F, Lenig D, Forster R, Lipp M, Lanzavecchia A. Two subsets of memory T lymphocytes with distinct homing potentials and effector functions. Nature 1999;401:708–12.

[37] Flynn JK, Gorry PR. Stem memory T cells (TSCM)-their role in cancer and HIV immunotherapies. Clin Transl Immunol 2014;3:e20.

[38] Klebanoff CA, Gattinoni L, Palmer DC, Muranski P, Ji Y, Hinrichs CS, et al. Determinants of successful CD8+ T-cell adoptive immunotherapy for large established tumors in mice. Clin Cancer Res 2011;17:5343–52.

[39] Sato K, Choyke PL, Kobayashi H. Photoimmunotherapy of gastric cancer peritoneal carcinomatosis in a mouse model. PLoS One 2014;9:e113276.

[40] Nagaya T, Nakamura Y, Sato K, Zhang YF, Ni M, Choyke PL, et al. Near infrared photoimmunotherapy with an anti-mesothelin antibody. Oncotarget 2016;7:23361–9.

[41] Nagaya T, Nakamura Y, Sato K, Harada T, Choyke PL, Kobayashi H. Near infrared photoimmunotherapy of B-cell lymphoma. Mol Oncol 2016;10:1404–14.

[42] Nagaya T, Nakamura Y, Sato K, Harada T, Choyke PL, Hodge JW, et al. Near infrared photoimmunotherapy with avelumab, an anti-programmed death-ligand 1 (PD-L1) antibody. Oncotarget 2017;8:8807–17.

[43] Watanabe R, Hanaoka H, Sato K, Nagaya T, Harada T, Mitsunaga M, et al. Photoimmunotherapy targeting prostate-specific membrane antigen: are antibody fragments as effective as antibodies? J Nucl Med 2015;56:140–4.